QUANTIFYING FOREST ABOVEGROUND BIOMASS USING REMOTE SENSING AND GROUND MEASUREMENTS FOR MIXED HARDWOOD FORESTS IN EAST TENNESSEE

Sakar Jha, Sheng-I Yang, D. Stuart Hale, David Shoch, Trisha Johnson, Donald G. Hodges, and Kevin P. Hoyt

ABSTRACT

Multispectral data collected from satellite-based sensors serve as a powerful tool for quantifying forest aboveground biomass. In this paper, we evaluated the performance of models that used satellite-image-derived variables and the models that used a combination of satellite-image-derived variables along with stand-level attributes to quantify forest aboveground biomass of natural mixed-hardwood forests. Imagery from Landsat 8 and Sentinel 2 satellite missions were used to derive the remote-sensing variables. We also identified the important predictors for these models using the recursive feature elimination method. The models that included variables derived from satellite images and stand-level attributes performed better than the models that only used variables derived from satellite images.

INTRODUCTION

Forest aboveground biomass (AGB) is quantified using *in situ* forest measurements, which are resource intensive to obtain (Flade and others 2020, Jones and others 2020). Multiple studies have been conducted for quantifying forest AGB using remote sensing as that technology has proven to be easier and more efficient (Csillik and others 2019, Deo and others 2017, Issa and others 2020). Satellite-based multispectral imagery is a cost-efficient alternative for quantifying AGB over a large area. The auxiliary information derived from satellite images captured from numerous satellite missions such as Landsat, Sentinel, and MODIS have all proved that they can quantify AGB at a reasonable precision. López-Serrano and others (2020), for example, used Landsat 8 images to model AGB in temperate forests of Mexico. Pandit and others (2020) used Sentinel 2 images to quantify AGB in the subtropical forests in Nepal. Blackard and others (2008) utilized MODIS data along with forest measurement data to produce the forest AGB map of the entire United States. Most of the studies that used multi-spectral imagery to quantify AGB only used predictors derived from them to model AGB. However, the AGB estimates provided by these models are not precise. To the best of our knowledge, no research has looked at combining stand-level attributes derived from ground-based measurements with variables derived from satellite imagery to quantify AGB in east Tennessee.

The aim of this project was to compare the accuracy and precision of AGB estimates produced by machine-learning models using only remote-sensing predictors and models combining remote-sensing predictors with stand-level attributes for natural mixed hardwood forests

Sakar Jha, Graduate Student, School of Natural Resources, University of Tennessee, Knoxville, TN 37996
Sheng-I Yang, Assistant Professor, School of Natural Resources, University of Tennessee, Knoxville, TN 37996
D. Stuart Hale, Forest Program Manager, US Carbon Markets Team, The Nature Conservancy, Arlington, VA 22203
David Shoch, Technical Director, TerraCarbon LLC, Charlottesville, VA 22902
Trisha Johnson, Senior Manager Operations, TerraCarbon LLC, Sparta, TN 38583
Donald G. Hodges, Professor and Director, School of Natural Resources, University of Tennesse, Knoxville, TN 37996
Kevin P. Hoyt, Center Director, Forest Resources AgResearch and Education Center, University of Tennessee, Knoxville, TN 37996

in east Tennessee. The models were built using the random forest algorithm, and the important variables were identified using the recursive feature elimination method.

METHODS

This study was carried out using forest carbon inventory data from four sites in east Tennessee (fig. 1). A total of 216 fixed-radius measurement plots were measured at four sites: Chestnut Mountain (n = 90), Oak Ridge (n = 29), Cumberland north (n = 57), and Cumberland south (n = 40). Additional details about sampling and measurement can be found in Yang and others (2022). These sites are largely composed of various species of maples (*Acer* spp.), oaks (*Quercus* spp.) and hickories (*Carya* spp.), with some shortleaf pines (*Pinus echinata*) and loblolly pines (*Pinus taeda*). The AGB of the trees was calculated using species-specific biomass equations published by Jenkins and others (2004). Mean tree height, trees/ha, and basal area (m^2/ha) were calculated for every plot.

Satellite images from Landsat 8 mission with operational land imager sensors and Sentinel 2 mission with multispectral imager sensors were downloaded for the sites during the leaf-on season. The images from both the satellite missions had a cloud cover of less than 5 percent. From these satellite images the blue, green, red, near infrared (NIR), and shortwave infrared 1 and 2 (SWIR 1 and SWIR 2) were extracted. Vegetation has high reflectance at NIR and low reflectance at the red region of the electromagnetic spectrum. Hence, the difference between these two bands describes the characteristics of vegetation. Using this property of vegetation, several vegetation indices have been derived from satellite images. In this study, six vegetation indices were calculated from the Landsat 8 and Sentinel 2 satellite images using the expressions in table 1. These

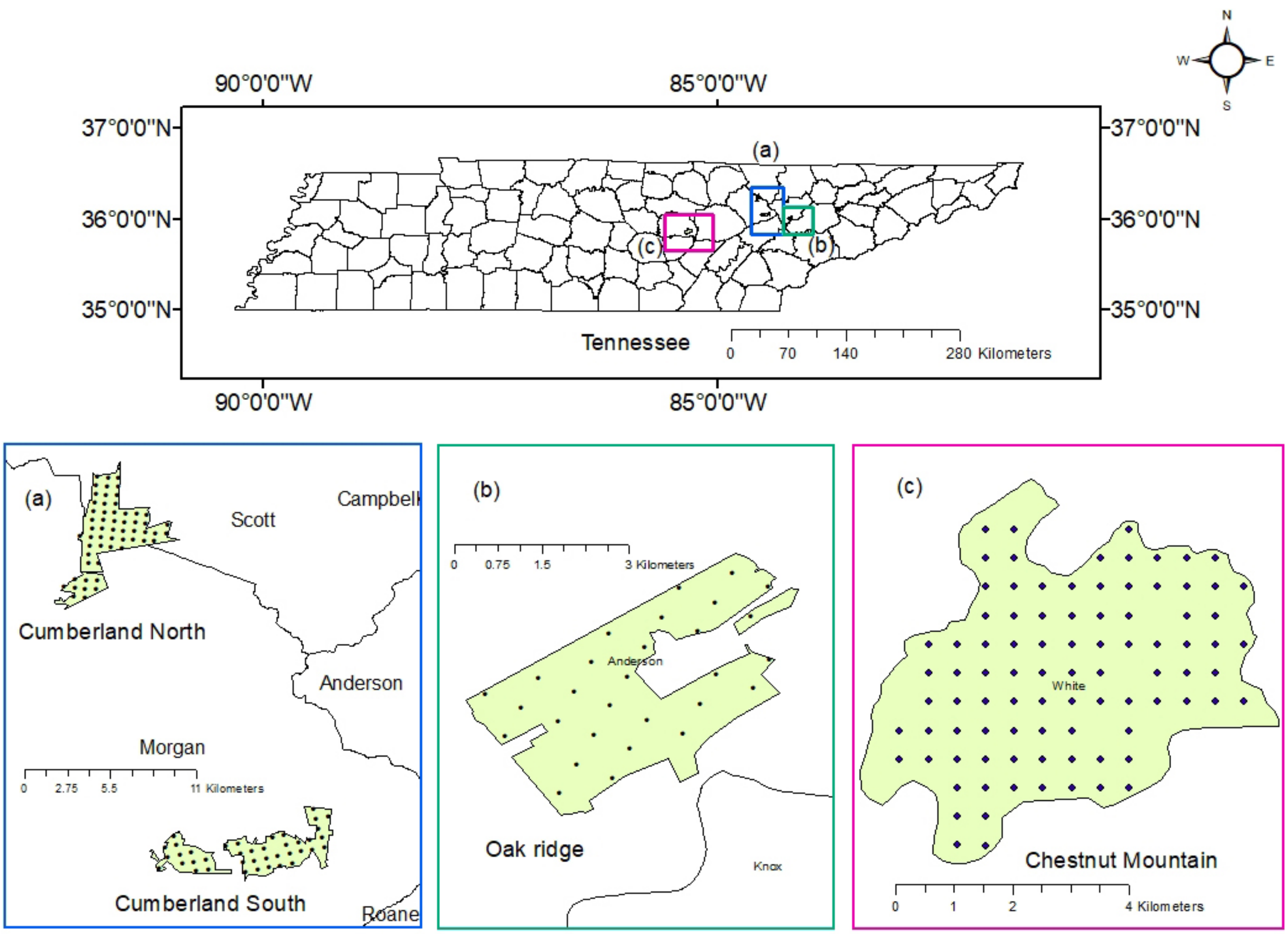

Figure 1—Map of the four study areas. Dots represent the location of forest measurement plots.

Table 1—Stand-level attributes and vegetation indices calculated from ground-based measurements and satellite images

Type	Variables	Expression	Reference
Stand-level attributes	TPH	Trees per hectare	–
	BA	Basal area (m^2/ha)	–
	Mean tree height	Average height of inventoried trees (m)	–
Spectral bands	Blue, Green, Red, NIR, SWIR-1, SWIR-2	–	–
Vegetation indices	Normalized difference vegetation index	(NIR-Red)/(NIR+Red)	Rouse 1974
	Soil-adjusted vegetation index	[(NIR-Red)/(NIR+Red+0.5)] *1.5	Huete 1988
	Enhanced vegetation index	2.5*((NIR-Red)/(NIR+6*Red-7.5*Blue) +1))	Huete and others 2002
	Atmospherically resistant vegetation index	(NIR-(Red-1*(Blue-Red)))/(NIR+(Red-1*(Blue-Red)))	Kaufman and Tanré 1992
	Ratio vegetation index	NIR/Red	Rondeaux and others 1996
	Difference vegetation index	NIR-Red	Tucker 1979

Blue = blue band; Green = green band; Red = red band; NIR = near infrared band; SWIR-1 and SWIR2 = shortwave infrared bands 1 and 2 from the satellite images.

vegetation indices were extracted from the pixels that directly correspond to each plot location. Similarly, texture metrics were calculated for each of the six satellite image bands from Landsat 8 and Sentinel 2 satellite images using the gray level co-occurrence matrix algorithm. Based on previous studies (Dube and Mutanga 2015, Li and others 2020, Pandit and others 2020), seven texture metrics (contrast, dissimilarity, mean, homogeneity, angular second moment, entropy, and variance) were calculated with a moving window size of 3 by 3 (table 2). Similar to vegetation indices, the values of texture metrics were extracted from the pixels that directly corresponded to each plot location.

Table 2—Expressions of seven texture metrics calculated from the satellite images as given by Haralick and others (1973)

Texture metric	Expression
Contrast	$\sum_{x,y=0}^{N-1} P_{x,y}(x-y)^2$
Dissimilarity	$\sum_{x,y=0}^{N-1} P_{x,y}\lvert x-y \rvert$
Mean	$\sum_{x,y=0}^{N-1} y(P_{x,y})$
Homogeneity	$\sum_{x,y=0}^{N-1} P_{x,y}/(1+(x-y)^2)$
Angular second moment	$\sum_{x,y=0}^{N-1} P_{x,y}^2$
Entropy	$\sum_{x,y=0}^{N-1} P_{x,y}(-\ln P_{x,y})$
Variance	$\sum_{x,y=0}^{N-1} P_{x,y}\,(y-\text{Mean})^2$

$P_{x,y}$ = the probability of reflectance value of pixel x and pixel y co-occurring in the moving window.
x and y = the reflectance value of a pixel x and pixel y in the moving window.
N = number of gray levels in the satellite band images.

The 6 spectral bands, 6 vegetation indices, 42 textural metrics, and 3 stand-level attributes were used to predict the AGB of the sites. The ground-based AGB calculated from the forest inventory data was used as the response variable. These variables were modeled using a random forest (RF) algorithm. It is a nonparametric approach to carrying out classification and regression problems, which employs bagging and boosting techniques to build decision trees (Breiman 2001). Within the RF algorithm, decision trees are created by randomly selecting two-thirds of the data to train the model, and the remaining one-third of the data to assess the model errors. Two sets of models were built for each satellite image (Landsat 8 and Sentinel 2): one using only satellite-image-derived variables as predictors and one using both satellite-image-derived variables and stand-level attributes.

The percent root mean square error (RMSE), percent mean bias (MB), and coefficient of determination (R^2) were calculated to evaluate the model performance. They were computed as:

$$RMSE(\text{percent}) = 100 * \sqrt{\sum_{k=1}^{n} \frac{((Y_k - \widehat{Y_k})/Y_k)^2}{n}} \quad (1)$$

$$MB(\text{percent}) = 100 * \sum_{k=1}^{n} \frac{(Y_k - \widehat{Y_k})}{n * Y_k} \quad (2)$$

$$R^2 = 1 - \frac{\sum_{k=1}^{n} (Y_k - \widehat{Y_k})^2}{\sum_{k=1}^{n} (Y_k - \bar{Y})^2} \quad (3)$$

where

Y_k is the observed AGB of plot k,

$\widehat{Y_k}$ is the predicted AGB of plot k,

$\bar{Y}$ is the average AGB from all plots, and

n is the number of plots.

To identify the important variables for each RF model, the recursive feature elimination (RFE) method was used. The RFE method iteratively selects a subset of predictors by eliminating the weakest predictor from the model until the subset with the lowest RMSE is reached. The RFE method was implemented using the 5-fold crossvalidation method to select the subset of predictor variables that produced the lowest RMSE.

RESULTS AND DISCUSSION

Performance of Models

Among the two sets of models, the model that used only variables extracted from the Landsat 8 satellite image as predictors performed better than the model that used only variables extracted from Sentinel 2 image (fig. 2). The Landsat-8-only

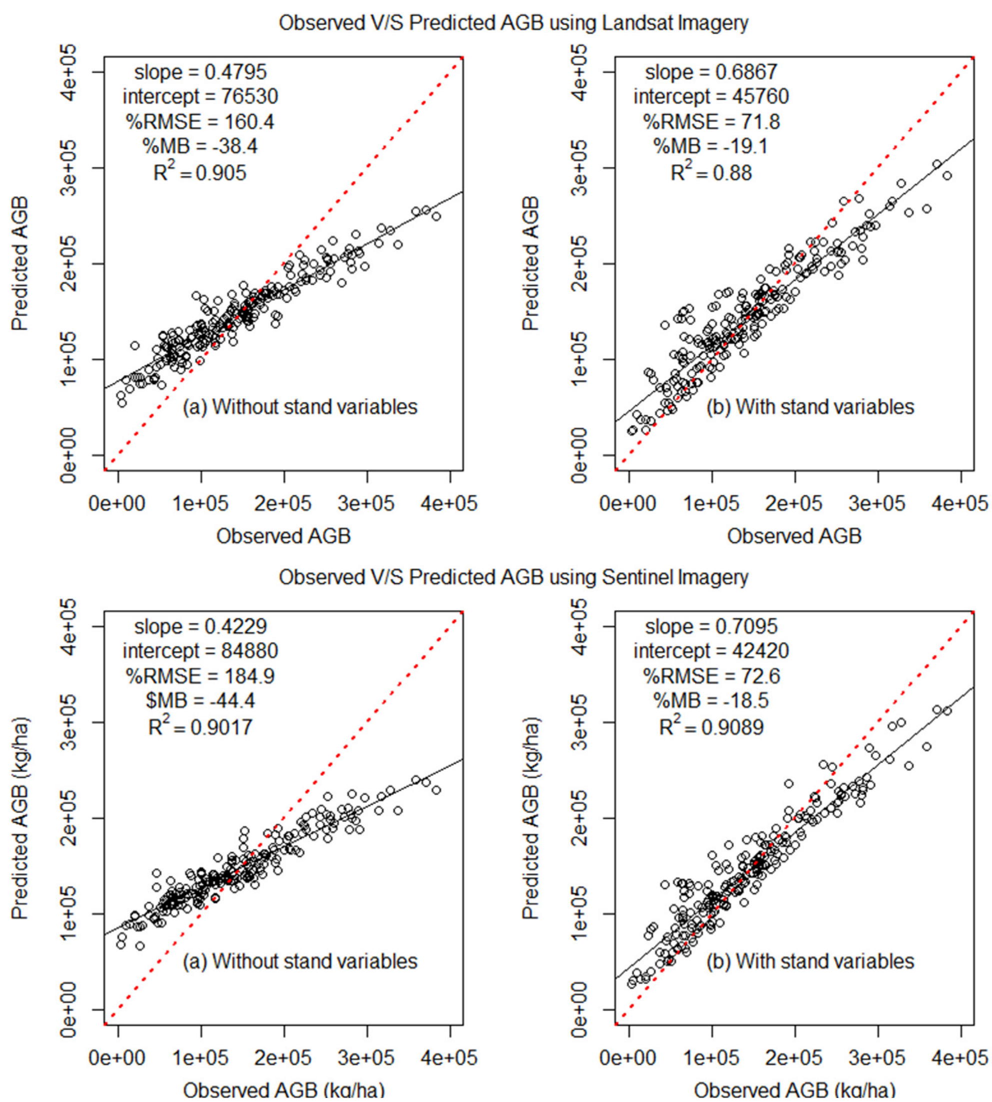

Figure 2—Observed versus predicted aboveground biomass (AGB) for the random forest models using Landsat 8 variables (top row) and Sentinel 2 variables (bottom row).

model had an RMSE of 160.4 percent and an MB of -38.4 percent, whereas the Sentinel-2-only model had a RMSE of 184.9 percent and MB of -44.4 percent. The slope of the best fit line between the observed and predicted AGB for the Landsat-8-only model was greater than that for the Sentinel-2-only model. When the remote-sensing variables were combined with stand-level attributes, the Sentinel 2 plus stand-level attributes model produced lower percent MB than Landsat 8 plus stand-level attributes model. The model with Sentinel 2 variables plus stand-level attributes had a RMSE of 72.6 percent and MB of -18.5 percent compared to 71.8 percent and -19.1 percent for the Landsat 8 plus stand-level attributes model. The slope of the best fit line between the observed and predicted AGB for Sentinel 2 plus stand-level attributes model was higher than that for the Landsat 8 plus stand-level attributes model. Figure 3 shows the spatial pattern of predicted aboveground biomass for the Sentinel 2 plus stand-level attributes model.

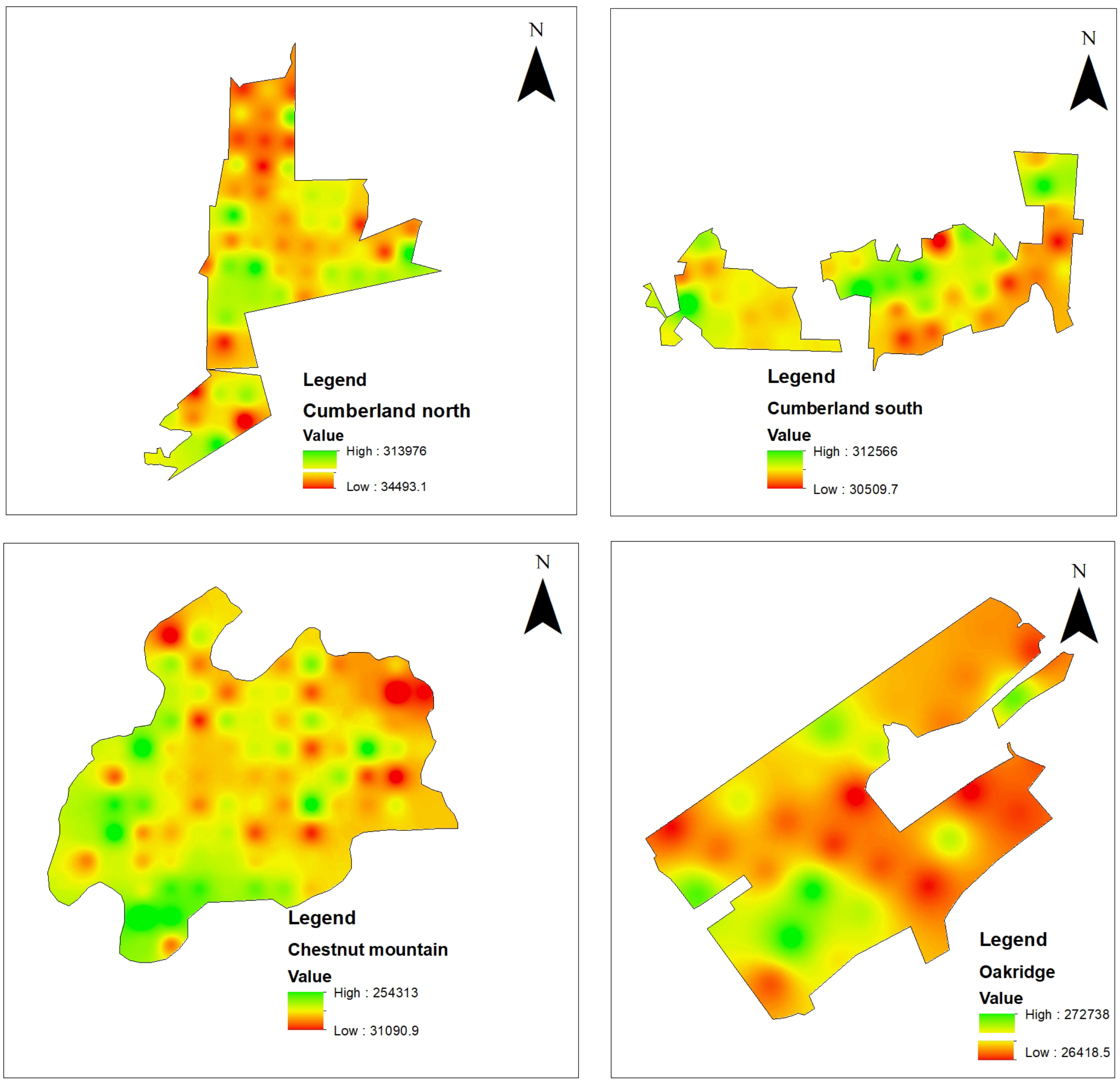

Figure 3—Spatial pattern of the predicted aboveground biomass for the Sentinel 2 plus stand-level attributes model for each of the four study areas. Areas with low aboveground biomass are shown in red, while areas with high aboveground biomass are shown in green.

Feature Importance

The RFE method selected a different subset of variables by removing the weakest feature for each of the four models (table 3). For the models with only remote-sensing variables, the texture metrics in green, blue, NIR, and SWIR bands were found to be more important than other vegetation indices and texture metrics. Among the seven different types of texture metrics, there was no clear pattern of one being more important than the rest. For models with both remote-sensing variables plus stand-level attributes, the stand-level attributes were more important, which were followed by texture metrics in green, blue, NIR, and SWIR bands. For the Sentinel-2-only model, 52 of the 54 variables were found to be important whereas for the Landsat-8-only model, only 10 of the variables were found to be important. Notably, in this study, stand-level attributes were calculated from field-obtained data. However, stand-level attributes can also be derived from active remote sensors, such as those developed from light detection and ranging (LiDAR) data. It would be worthwhile for further studies to evaluate the impact of stand-level attributes computed from different approaches on AGB estimation.

CONCLUSIONS

Inclusion of stand-level attributes as predictors along with remote-sensing variables can improve the estimation of forest AGB. The Landsat-8-only model performed better than the Sentinel-2-only model. When stand-level attributes are included, the Sentinel 2 plus stand-level attributes model performed better than the Landsat 8 plus stand-level attributes model. Texture metrics are important remote-sensing predictors for estimating AGB, particularly texture metrics of green, blue, NIR, and SWIR bands.

REFERENCES

Blackard, J.A.; Finco, M.V.; Helmer, E.H. [and others]. 2008. Mapping U.S. forest biomass using nationwide forest inventory data and moderate resolution information. Remote Sensing of Environment. 112(4): 1658–1677. https://doi.org/10.1016/j.rse.2007.08.021.

Breiman, L. 2001. Random forests. Machine Learning. 45: 5–32.

Csillik, O.; Kumar, P.; Mascaro, J. [and others]. 2019. Monitoring tropical forest carbon stocks and emissions using Planet satellite data. Scientific Reports. 9: 17831 12 p. https://doi.org/10.1038/s41598-019-54386-6.

Deo, R.K.; Russell, M.B.; Domke, G.M. [and others]. 2017. Evaluating site-specific and generic spatial models of aboveground forest biomass based on Landsat time-series and LiDAR strip samples in the eastern USA. Remote Sensing. 9: 598. 23 p. https://doi.org/10.3390/rs9060598.

Dube, T.; Mutanga, O. 2015. Investigating the robustness of the new Landsat-8 Operational Land Imager derived texture metrics in estimating plantation forest aboveground biomass in resource constrained areas. ISPRS Journal of Photogrammetry and Remote Sensing. 108: 12–32. https://doi.org/10.1016/j.isprsjprs.2015.06.002.

Flade, L.; Hopkinson, C.; Chasmer, L. 2020. Allometric equations for shrub and short-stature tree aboveground biomass within boreal ecosystems of northwestern Canada. Forests. 11: 1207. 16 p. https://doi.org/10.3390/f11111207.

Haralick, R.M.; Shanmugam, K.; Dinstein, I. 1973. Textural features for image classification. IEEE Transactions on Systems, Man, and Cybernetics. SMC-3(6): 610–621. https://doi.org/10.1109/TSMC.1973.4309314.

Huete, A.; Didan, K.; Miura, T. [and others]. 2002. Overview of the radiometric and biophysical performance of the MODIS vegetation indices. Remote Sensing of Environment. 83: 195–213. https://doi.org/10.1016/S0034-4257(02)00096-2.

Table 3—Optimal predictors indentified for the four models using the recursive feature elimination method

Models	Optimal variables
Landsat 8 only	variance_green, green, homogeneity_IR, mean_green, second_moment_IR, mean_blue, SWIR1, variance_blue, dissimilarity_IR, homogeneity_green
Landsat 8 plus stand-level attributes	BA, Mean tree height, TPH, variance_green, green, mean_blue
Sentinel 2 only	contrast_SWIR2, green, dissimilarity_SWIR2, entropy_SWIR1, entropy_IR, homogeneity_SWIR1, second_moment_SWIR1, second_moment_IR, contrast_SWIR1, entropy_SWIR2, entropy_Red, second_moment_SWIR2, variance_red, blue, entropy_green, mean_red, dissimilarity_SWIR1, second_moment_green, mean_SWIR2, mean_green, homogeneity_IR, variance_green, red, homogeneity_SWIR2, contrast_IR, contrast_red, variance_SWIR2, entropy_blue, variance_blue, second_moment_red, dissimilarity_red, homogeneity_red, contrast_green, arvi, SWIR2, evi, rvi, dissimilarity_IR, second_moment_blue, homogeneity_blue, mean_IR, savi, ndvi, mean_blue, homogeneity_green, variance_SWIR1, dissimilarity_blue, IR, contrast_blue, SWIR1, mean_SWIR1, variance_IR, dissimilarity_green
Sentinel 2 plus stand-level attributes	BA, Mean tree height, entropy_IR, TPH, second_moment_IR, mean_SWIR1

TPH = trees/ha; BA = basal area (m^2/ha).

Huete, A.R. 1988. A soil-adjusted vegetation index (SAVI). Remote Sensing of the Environment. 25: 295–309. https://doi.org/10.1016/0034-4257(88)90106-X.

Issa, S.; Dahy, B.; Ksiksi, T.; Saleous, N. 2020. A review of terrestrial carbon assessment methods using geo-spatial technologies with emphasis on arid lands. Remote Sensing. 12: 2008. 32 p. https://doi.org/10.3390/rs12122008.

Jenkins, J.C.; Chojnacky, D.C.; Heath, L.S.; Birdsey, R.A. 2004. Comprehensive database of diameter-based biomass regressions for North American tree species. Gen. Tech. Rep. NE-319. Newtown Square, PA: U.S. Department of Agriculture Forest Service, Northeastern Research Station. 45 p. https://doi.org/10.2737/NE-GTR-319.

Jones, A.R.; Raja Segaran, R.; Clarke, K.D. [and others]. 2020. Estimating mangrove tree biomass and carbon content: a comparison of forest inventory techniques and drone imagery. Frontiers in Marine Science. 6: 784. 13 p. https://doi.org/10.3389/fmars.2019.00784

Kaufman, Y.J.; Tanré, D. 1992. Atmospherically resistant vegetation index (ARVI) for EOS-MODIS. IEEE Transactions on Geoscience and Remote Sensing. 30(2): 261–270. https://doi.org/10.1109/36.134076.

Li, Y.; Li, M.; Li, C.; Liu, Z. 2020. Forest aboveground biomass estimation using Landsat 8 and Sentinel-1A data with machine learning algorithms. Scientific Reports. 10: 9952. 12 p. https://doi.org/10.1038/s41598-020-67024-3

López-Serrano, P.M.; Domínguez, J.L.C.; Corral-Rivas, J.J. [and others]. 2020. Modeling of aboveground biomass with Landsat 8 OLI and machine learning in temperate forests. Forests. 11: 11. 18 p. https://doi.org/10.3390/f11010011.

Pandit, S.; Tsuyuki, S.; Dube, T. 2020. Exploring the inclusion of Sentinel-2 MSI texture metrics in above-ground biomass estimation in the community forest of Nepal. Geocarto International. 35(16): 1832–1849. https://doi.org/10.1080/10106049.2019.1588390.

Rondeaux, G.; Steven, M.; Baret, F. 1996. Optimization of soil-adjusted vegetation indices. Remote Sensing of Environment. 55(2): 95–107. https://doi.org/10.1016/0034-4257(95)00186-7.

Rouse, J.W., Jr. 1974. Monitoring the vernal advancement of retrogradation (green wave effect) of natural vegetation. Type 1 Progress Report Number 7. College Station, TX: Texas A&M University, Remote Sensing Center. 8 p. https://ntrs.nasa.gov/api/citations/19740022555/downloads/19740022555.pdf.

Tucker, C.J. 1979. Red and photographic infrared linear combinations for monitoring vegetation. Remote Sensing of the Environment. 8: 127–150. https://doi.org/10.1016/0034-4257(79)90013-0.

Yang, S.; Cao, Q.V.; Shoch, D.T.; Johnson, T. 2022. Characterizing stand and biomass tables from diameter distribution models: a case study for mixed-hardwood forests in eastern Tennessee, USA. Forest Science. 68(1): 8–16. https://doi.org/10.1093/forsci/fxab051.